International Journal of Solids and Structures 49 (2012) 1022–1032

Contents lists available at SciVerse ScienceDirect

International Journal of Solids and Structures

journal homepage: www.elsevier.com/locate/ijsolstr

Finite Fracture Mechanics at elastic interfaces

P. Cornetti [a,*], V. Mantič [b], A. Carpinteri [a]

[a] Department of Structural Engineering and Geotechnics, Politecnico di Torino, Corso Duca degli Abruzzi 24, 10129 Torino, Italy
[b] Group of Elasticity and Strength of Materials, School of Engineering, University of Seville, Camino de los Descubrimientos s/n, 41092 Seville, Spain

ARTICLE INFO

Article history:
Received 25 July 2011
Received in revised form 9 November 2011
Available online 17 January 2012

Keywords:
Finite Fracture Mechanics
Elastic interfaces
Double lap joint
Cohesive crack model

ABSTRACT

In the present paper we provide a method to determine the load causing delamination along an interface in a composite structure. The method is based on the elastic interface model, according to which the interface is equivalent to a bed of linear elastic springs, and on Finite Fracture Mechanics, a crack propagation criterion recently proposed for homogeneous structures. The procedure outlined is general. Details are given for the pull–push shear test. For such geometry, the failure load is obtained and compared with the estimates provided by stress concentration analysis and Linear Elastic Fracture Mechanics. It is seen that Finite Fracture Mechanics provides intermediate values. Furthermore, it is shown that the predictions provided by Finite Fracture Mechanics are almost coincident with the ones provided by the Cohesive Crack Model. As far as we are concerned with the determination of the failure load, the advantage of using Finite Fracture Mechanics with respect to the Cohesive Crack Model is evident, since a troublesome analysis of the softening taking place in the fracture process zone is not necessary. A final comparison with classical fracture criteria based on critical distances, such as the average stress criterion, concludes the paper.

1. Introduction

In bonded joints as well as in composite structures, the modeling of the interfaces is of primary concern, since one of the most common failures is the debonding of one component from the others. In fact, for small values of applied loads, the glue guarantees the bonding of the junction, although a jump of displacements is allowed due to the compliance of the interface. If the loads increase, however, it may happen that the adhesive breaks in one or more points and that a crack initiates and then propagates along the interface leading finally to the complete detachment of the adherents.

In many practical situations, the mechanical behavior of the interface can be described by assuming that the adherents are joined along the common part of their boundary by a continuous distribution of linear springs of adequate stiffness, which simulate the presence of the adhesive (see Lenci (2001) for a review). Note that the behavior of this interface model is equivalent to that of a thin, soft, elastic layer in the limit when the layer thickness and stiffness both approach zero. It is usually referred to as (linear) *elastic interface*, *weak interface* or *imperfect interface* model and its first application dates back to the work by Volkersen (1938) and Goland and Reissner (1944). With respect to the *strong interface* model (i.e. perfect bonding), it can be handled in a relatively simpler way, and for some geometries it leads to analytical results. On the other hand, the strong interface model yields stress singularities which become oscillating in case of a crack between dissimilar materials (Williams, 1959; England, 1965; Rice and Sih, 1965; Rice, 1988). In such a case even the definition of mode mixity results troublesome.

The aim of the present paper is to provide a way to determine the load causing delamination along a weak interface based on Finite Fracture Mechanics (FFM), recently introduced by Leguillon (2002) and Cornetti et al. (2006). Note that FFM has already been applied successfully to interface problems by exploiting a multi-scale approach (Leguillon et al., 2003), i.e. modeling the adhesive as a full 2D elastic medium at the micro-scale and as a strong interface at the macro-scale. Of course, such an approach is much more sophisticated than the one proposed here, but our goal is to provide an easy although sufficiently accurate model able to provide recommendations and formulae that can be useful in engineering practice when delamination problems arise. Finally, let us mention that, during the revision process, we became aware of the work by Weißgraeber and Becker (2011) developing an approach similar to the one proposed here.

In the following section the general procedure is outlined, while, in the remaining sections, a benchmark geometry, i.e. the pull–push shear test, is investigated to highlight the capabilities of the method. Comparisons with other models available in literature conclude the paper, showing the advantages of the proposed approach.

* Corresponding author.
E-mail address: pietro.cornetti@polito.it (P. Cornetti).

0020-7683/$ - see front matter © 2012 Elsevier Ltd. All rights reserved.
doi:10.1016/j.ijsolstr.2012.01.002

2. Cracks at weak interfaces

Weak interfaces are commonly used to model the interphase or the adhesive layer between two materials. This approach is rigorous only for vanishing adhesive thicknesses; furthermore the adhesive elastic moduli have to tend to zero exactly as the thickness goes to zero. Under these circumstances, denoting by E_a, G_a and h_a the Young's modulus, the shear modulus and the thickness of the adhesive layer, respectively, the interphase can be modeled as a bed of springs normal and tangent to the interface, with stiffnesses $k_n = E_a/h_a$ and $k_t = G_a/h_a$, respectively. Across a weak interface, therefore, tractions are continuous but displacement jumps are possible. A detailed proof of these results can be found in Klarbring (1991) and Bigoni et al. (1998), the latter considering also anisotropic interphases. The simplicity of the model is the cause of its wide spreading in the scientific literature (see, e.g., Benveniste and Miloh, 2001; Hashin, 2002).

Since adhesives are soft and the adhesive layers are thin, the two previous assumptions are approximately met when dealing with bonded joints. Nevertheless, it should be observed that the weak interface model is a (first) approximation to the real behavior of adhesive layers and therefore it misses some aspects of the problem that may be relevant in some cases: for instance, it cannot catch non-uniform stress distributions across the adhesive thickness as well as the coupling between shear and normal stresses within the elastic adhesive layer. Such features can be caught by higher-order models; a comparison between the weak interface model and a 2D description of the adhesive layer can be found, for instance, in Rabinovitch (2004) for a specific geometry (a three point bending beam strengthened by a plate at its intrados).

Before analyzing the crack propagation along a weak interface, it is worth highlighting some differences between the case of perfect bonding (i.e. a strong interface) – see Fig. 1a – and that of the weak interface – see Fig. 1b. For the sake of clarity, in Fig. 1 we consider an edge crack of length a placed along the interface between the two adherents; moreover, for the sake of simplicity, we assume that the crack is subjected only to a mode I loading.

If the two adherents (either perfectly or weakly bonded) are made of the same material, the strong interface case corresponds to a crack in a homogeneous medium. In such a case it is well known that no displacement discontinuity may appear across the x-axis ahead of the crack tip while the stress field is singular, its asymptotical expression being $\sigma_y(x) = K_I/\sqrt{2\pi(x-a)}$, where K_I is the stress-intensity factor. On the other hand, if we consider the weak interface case (i.e. a bed of linear springs, normal to the interface, of stiffness k_n), a displacement discontinuity v takes place because of the interface compliance, whereas the stresses, linked to the displacement by the linear relationship $\sigma_y = k_n\, v$, remain finite along the interface. Usually, the maximum stress is achieved at the crack tip, i.e. $\sigma_{max} = \sigma_y(a)$.

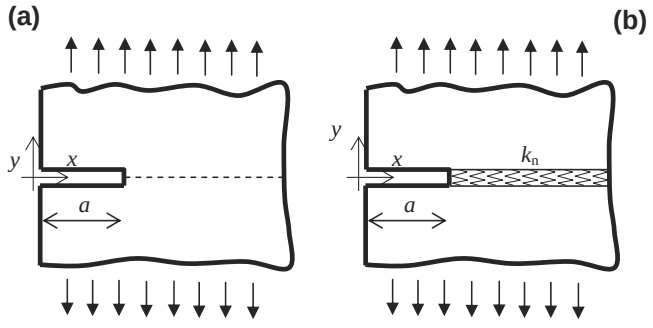

Fig. 1. Edge crack along a strong (a) and weak (b) interface.

Assuming a brittle behavior of the material and of the interface, we can apply Linear Elastic Fracture Mechanics (LEFM). To this aim, one needs to evaluate the strain energy release rate $\mathcal{G}$. While for the crack in a homogeneous medium the strain energy release rate is given by the well-known Irwin's relationship ($\mathcal{G} = K_I^2/E$, E being the Young's modulus of the material), in the elastic interface geometry the strain energy release rate equals the strain energy stored in the spring ahead the crack tip (Lenci, 2001), i.e.:

$$\mathcal{G} = \frac{\sigma_{max}^2}{2k_n} \tag{1}$$

According to LEFM, the crack propagates as soon as the strain energy release rate $\mathcal{G}$ reaches the mode I fracture energy $\mathcal{G}_{Ic}$. For the strong interface case, this condition occurs when the stress intensity factor K_I reaches the material fracture toughness K_{Ic}; for the weak interface case, Eq. (1) shows it occurs when:

$$\sigma_{max} = \sqrt{2k_n\mathcal{G}_{Ic}} \tag{2}$$

where now $\mathcal{G}_{Ic}$ represents the mode I fracture energy of the interface. Eq. (2) clearly shows that the LEFM criterion can be written in term of stresses if the crack is located along a weak interface.

Eqs. (1) and (2) have been exploited by Lenci (2001) to address the problem of two elastic half-planes joined along the common part of their boundary by a cracked weak interface (Fig. 2). Note that this geometry contains as a particular case, i.e. neglecting the interface compliance ($k_n \to \infty$), the classical Griffith crack in a homogeneous medium. Furthermore, Lenci (2001) showed that the strain energy release rate obtained by Eq. (1) is higher than the estimate obtained by Irwin's relationship $\mathcal{G} = K_I^2/E$ for the Griffith crack (the two values merge for infinitely long cracks): it means that the strong interface model provides higher failure loads with respect to the weak interface model and, consequently, neglecting the interface compliance is potentially dangerous. Although this trend is not a general property, it holds true for several geometries of practical interest, such as, e.g., the double cantilever beam test (Kanninen, 1973), the pull–push shear test (see next section) or the plate debonding of externally reinforced beam (provided that the reinforcement length is large enough, see Carpinteri et al. (2009) for details).

Another important difference between strong and weak interfaces is that, while in a homogeneous medium LEFM *cannot* be used to predict crack initiation since $K_I \to 0$ as $a \to 0$ (thus providing an infinite failure load), for a vanishing crack along a weak interface LEFM *can* be used, at least in principle. In fact, generally, the maximum stress remains finite (and larger than zero) even if there is no crack.

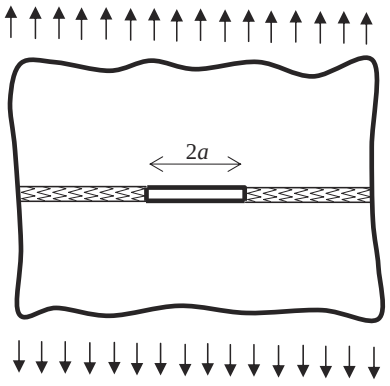

Fig. 2. Two elastic half-planes joined along the common part of their boundary by a cracked weak interface.

Despite this positive feature, it is easily argued that, in the case of short or no cracks and in the case of quasi-brittle interfacial behavior (i.e. not perfectly brittle interfaces), more accurate failure load predictions can be achieved only by considering, beyond the interface fracture energy, the interfacial strength σ_p. To this aim, we may resort to Finite Fracture Mechanics. Following the approach outlined in Cornetti et al. (2006), under a mode I load, a crack propagates by a finite crack extension Δ if the following two inequalities are satisfied:

$$\begin{cases} \int_a^{a+\Delta} \sigma_y(x,a)\,dx \geqslant \sigma_p \Delta \\ \int_a^{a+\Delta} \mathcal{G}(a')\,da' \geqslant \mathcal{G}_{Ic}\Delta \end{cases} \tag{3}$$

The former inequality is a (average) stress requirement for crack to propagate, whereas the latter is an energy balance. It means that fracture is energy driven, but a sufficiently high stress field must act at the crack tip to trigger crack propagation. It is worth observing that, in the usual case (the so-called positive geometries) of monotonically increasing strain energy release rate $\mathcal{G}(a')$ and of monotonically decreasing stress $\sigma_y(x)$, the lowest failure load (i.e. the actual one) is attained when the two inequalities are substituted by the two corresponding equations. In fact, for positive geometries, the second inequality is satisfied for crack steps larger than a threshold value, thus providing a lower bound for the set of admissible Δ-values; on the contrary, the first inequality is satisfied for crack advancements smaller than a certain value, thus providing an upper bound. For low load values, the upper bound is smaller than the lower bound and, consequently, the set of admissible Δ-values is empty. As the external load increases, the upper bound increases and the lower bound decreases till a load value is met (i.e. the failure load) for which both conditions are strictly fulfilled. Therefore, we conclude stating that, for positive geometries, the system (3) reverts to a system of two equations in two unknowns: the (minimum) failure load and the corresponding crack advancement Δ.

In the strong interface case (Fig. 1a), we can exploit Irwin's relationship to get the following expression for the FFM criterion:

$$\begin{cases} \int_a^{a+\Delta} \sigma_y(x,a)\,dx = \sigma_p \Delta \\ \int_a^{a+\Delta} \frac{K_I^2(a')}{E}\,da' = \mathcal{G}_{Ic}\Delta \end{cases} \tag{4}$$

On the other hand, Eq. (1) can be used to particularize the application of the FFM criterion (3) to the debonding along a weak interface:

$$\begin{cases} \int_a^{a+\Delta} \sigma_y(x,a)\,dx = \sigma_p \Delta \\ \int_a^{a+\Delta} \frac{\sigma_y^2(x=a',a')}{2k_n}\,da' = \mathcal{G}_{Ic}\Delta \end{cases} \tag{5}$$

It is worth observing that, differently from Eq. (4), in the two equations of system (5) the same function appears, i.e. the stress field ahead of the crack tip. However note that, in the first equation, the integral is taken with respect to the spatial coordinate x, whereas, in the second equation, integration is performed with respect to the crack length a'.

The extension of the FFM criterion to delamination problem under mode II loading condition is straightforward. In fact, in such a case (Leung and Yang, 2006; Carpinteri et al., 2009), the strain energy release rate is simply given by:

$$\mathcal{G} = \frac{\tau_{max}^2}{2k_t} \tag{6}$$

where τ_{max} is the maximum shear stress, i.e. the shear stress at the crack tip, and k_t is now the stiffness of the tangential springs used to model the interface. Denoting with τ_p the shear strength and with $\mathcal{G}_{IIc}$ the mode II fracture energy, the FFM criterion now reads:

$$\begin{cases} \int_a^{a+\Delta} \tau(x,a)\,dx = \tau_p \Delta \\ \int_a^{a+\Delta} \frac{\tau^2(x=a',a')}{2k_t}\,da' = \mathcal{G}_{IIc}\Delta \end{cases} \tag{7}$$

Before proceeding, further comments about Eqs. (1) and (6) may be useful: (i) They generalize to weak interfaces the Irwin's relations for crack in homogeneous media, $\mathcal{G} = K_I^2/E$ and $\mathcal{G} = K_{II}^2/E$ for mode I and mode II respectively; (ii) Despite their physical meaning being evident (the strain energy release rate is the energy stored in the spring ahead the crack tip), their rigorous proof can be given by computing the crack closure work, as done in Carpinteri et al. (2009) to derive Eq. (6); (iii) Although elastic interfaces have been widely exploited to derive LEFM models, it seems that the knowledge of Eqs. (1) and (6) inside the scientific community is still limited and most of the authors compute the strain energy release rate by deriving the strain energy of the whole structure with respect to the crack length at constant load, i.e. by a procedure which is general but usually much more complicated than applying Eqs. (1) and (6) (see, e.g., Kanninen, 1973; Rabinovitch, 2004); (iv) If debonding occurs in mixed mode, the interface must be modeled by means of normal and tangential springs, so that the strain energy release rate is given by:

$$\mathcal{G} = \frac{\sigma_{max}^2}{2k_n} + \frac{\tau_{max}^2}{2k_t} \tag{8}$$

which can be also used to determine the mode mixity, as done by Bennati et al. (2009), where a LEFM model for the delamination in an asymmetric double cantilever beam has been developed, see also Távara et al. (2010, 2011).

Eq. (8) together with a suitable strength criterion under combined normal and tangential loads (see, e.g., Hebel et al. (2010) or Andersons et al. (2010) for FFM applied to strong interfaces) represent the key to extend the present approach to mixed mode delamination. However we will not pursue this goal in the present paper; it will be the subject of a future research. On the other hand, in the following section, the general procedure outlined above will be applied to a benchmark geometry, i.e. the pull–push shear test. This geometry has been chosen because of its relative simplicity: for such a test, under some simplifying assumptions, several fracture criteria can be implemented analytically so that the failure load predictions provided by FFM can be compared with those provided by easier (e.g., the average stress) or more sophisticated (e.g., the cohesive crack model) criteria.

For the pull–push shear test, delamination occurs in prevailing mode II conditions; hence we will apply FFM as provided by Eq. (7). In such a case, dimensional analysis arguments indicate that the solution must depend on the dimensionless parameter μ defined as:

$$\mu = \frac{2k_t\mathcal{G}_{IIc}}{\tau_p^2} \tag{9}$$

which rules the brittleness/ductility of the interface (it would have been equal to $2k_n\mathcal{G}_{Ic}/\sigma_p^2$ for a mode I delamination). Its meaning and range of validity is evident if we consider an interface whose mechanical behavior is described by a cohesive law with a linear softening (see Fig. 3), for which μ is also equal to the ratio between the displacement s_f (the value of the slip at which debonding occurs) and the displacement s_p (the value of the slip at the peak stress τ_p). Hence μ must be larger than unity: $\mu = 1$ corresponds to a linear elastic-perfectly brittle interface, whereas $\mu \to \infty$ implies a linear elastic-perfectly plastic interfacial behavior. Finally notice that, for $\mu = 1$, the energy condition for crack propagation ($\mathcal{G} = \mathcal{G}_{IIc}$) coincides with the attainment of the peak strength at the crack tip ($\tau_{max} = \tau_p$). It means that, for a linear elastic-perfectly brittle interface, the crack advancement provided by the system (7) is zero, i.e. the crack grows by infinitesimally small steps and FFM reverts to classical LEFM.

Recalling that the tangential stiffness k_t is given by the ratio of G_a to h_a, the mechanical condition $\mu \geqslant 1$ can also be expressed in

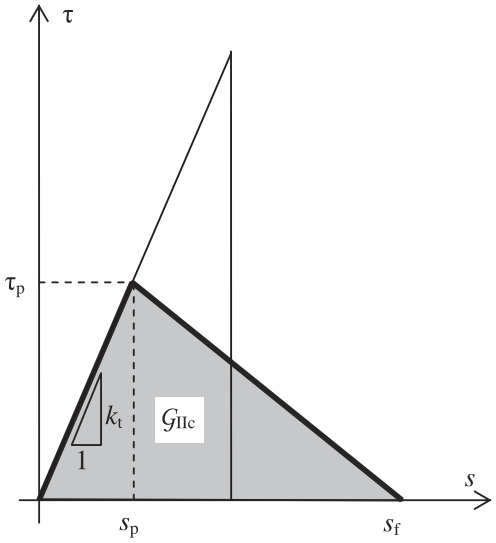

Fig. 3. Mode II cohesive law for an interface with linear softening (thick line, $\mu = s_f/s_p > 1$). The thin line corresponds to a linear elastic-perfectly brittle interface behavior with the same stiffness and fracture energy of the cohesive model ($\mu = 1$).

terms of the adhesive thickness, i.e. the weak interface model can be used as far as $h_a \leqslant h_{th}$, the threshold thickness h_{th} being equal to:

$$h_{th} = \frac{2G_a\mathcal{G}_{IIc}}{\tau_p^2} \tag{10}$$

From Eq. (10) it is evident that the threshold thickness is proportional to the plastic radius which develops in front of a crack (under mode II loading) in a specimen made of the adhesive material. Furthermore, by Eq. (10) it is also possible to express the dimensionless interfacial parameter μ as the ratio of the threshold thickness to its actual value, i.e. $\mu = h_{th}/h_a$. Thus, the present approach is applicable for sufficiently thin adhesive layers only. In this sense h_{th} defines the concept of *thin adhesive layer*. It should be noticed that in the limit case $h = h_{th}$ the present case reverts to LEFM on elastic interfaces with an infinitesimal crack advance, as developed by Bennati et al. (2009) and Távara et al. (2010, 2011).

One may wonder why the present approach can be applied only to structures where the adhesive thickness is smaller than a threshold value. In our opinion this might be because the simple continuous spring model, which assumes a homogeneous stress state in each spring, is not adequate for thick layers, where the assumption of the homogenous stress state along the thickness is not valid. In particular, if a spring is broken, all its strain energy is released. However, if the crack advances a bit, not all the strain energy in the thick adhesive layer above and below the crack step will be released. In such a case, it is argued that a full 2D description of the adhesive layer would be necessary to determine the strain energy release rate.

Finally it is interesting to see what happens for non-positive geometries. With reference to system (3), the function $\mathcal{G}(a')$ is decreasing (for $a' > a$); therefore the second inequality can be fulfilled only if $\mathcal{G}(a)$ is larger than or equal to $\mathcal{G}_{Ic}$. It is easily realized that the (minimum) failure load is attained exactly when $\mathcal{G}(a)$ is equal to $\mathcal{G}_{Ic}$, i.e. when the crack advancement Δ is equal to zero. In fact, for these values, the first inequality is always fulfilled, either we consider a crack in a homogeneous medium or a crack along an elastic interface: in the former case, the average stress over Δ is infinite as $\Delta \to 0$ since the stress field is singular; in the latter case, the maximum stress is equal to $\sqrt{2k_n\mathcal{G}_{Ic}}$ which is higher than σ_p because μ is larger than unity. Since Δ is equal to zero, we conclude that, for non-positive geometries, FFM reverts to LEFM. In the following, however, we will refer only to positive geometries, letting the analysis of failure processes where the strain energy release rate is decreasing or starts to decrease after a given crack length (e.g., because of a fundamental change in the global load resisting mechanism) to future researches.

3. The pull–push shear test

In Fig. 4 the (double) pull–push shear test is shown. It can be regarded as a kind of double lap joint. In such a joint, the adhesive layer is mainly subjected to shear deformations, so that delamination occurs in prevailing mode II conditions. However, note that a rigorous elastic analysis of the problem shows that also a mode I component is present (Suo and Hutchinson, 1990), but we will neglect such a contribution since peeling stresses are usually lower than shearing stresses. Furthermore, the smaller is the thickness of the outer adherents, the lower in absolute value and the more localized at the joint edges are the peeling stresses (Hart-Smith, 1973; Da Silva et al., 2009). From the previous considerations, we conclude that in several cases of practical interest, like fibre reinforced polymer (FRP) plates bonded to a concrete beam, peeling stresses can effectively be neglected. For the sake of simplicity we will refer to concrete and FRP in the following, although the equations hold for other materials as well. Note that in structural retrofitting the elastic interface model is rather common; see, e.g., Bruno and Greco (2001) and Rabinovitch (2004).

The aim of the present and next sections is to apply FFM to the analysis of the pull–push shear test. It is worth observing that the use of FFM makes the hypothesis of considering only shear stresses even more acceptable, since the effect of peeling stresses on the average stress condition is very low due to their highly localized nature; analogous result holds for the energy balance, where the strain energy of the normal and tangential springs are proportional to the square of their respective stresses (see Eq. (8)).

Referring to Fig. 4, we assume that the width and thickness of the FRP plate and of the concrete prism are constant along the length. The width and thickness of the reinforcement plate are denoted respectively by t_r and h_r, those of the concrete prism by t_b and $2h_b$, and the bonded length is denoted by l; x is the longitudinal coordinate. The Young's moduli of plate and concrete are E_r and E_b respectively.

According to the previous considerations, a simple mechanical model for the pull–push shear test can be established by treating

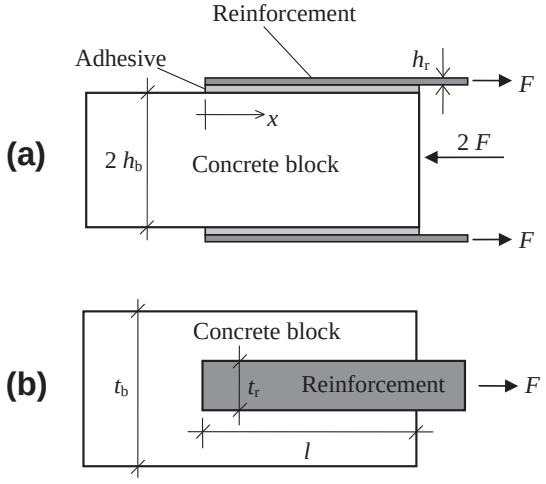

Fig. 4. Double pull–push shear test: (a) elevation; (b) plan.

the plate and the concrete prism (the two adherents) as being subjected to axial deformations only, while the adhesive layer (i.e. the interface) can be assumed to be subjected to shear deformations only. That is, both adherents are assumed to be subjected to uniformly distributed axial stresses, with any bending effects neglected, while the adhesive layer is modeled as a bed of horizontal springs with stiffness k_t (i.e. as a weak interface). Note that the assumption of uniformly distributed axial stress is valid only if the concrete block and the reinforcement have about the same width, which is therefore a further limitation to the present, simplified analysis. On the other hand, it is worthy observing that, since the adhesive layer is subjected to shear deformation only, the present model falls within the shear lag or Volkersen-type models.

Because of symmetry, we can consider only the upper half of the specimen (Fig. 5). Based on the previous assumptions, the equilibrium equations of the reinforcement and of the overall specimen cross section read respectively:

$$h_r \frac{d\sigma_r}{dx} - \tau = 0 \tag{11}$$

$$\sigma_r h_r t_r + \sigma_b h_b t_b = 0 \tag{12}$$

where τ is the shear stress in the adhesive layer, σ_r is the axial stress in the reinforcement plate and σ_b is the axial stress in the concrete prism. The constitutive equations for the adhesive layer and the two adherents are:

$$\tau = k_t s \tag{13}$$

$$\sigma_r = E_r \frac{du_r}{dx} \tag{14}$$

$$\sigma_b = E_b \frac{du_b}{dx} \tag{15}$$

where u_r and u_b are the longitudinal displacements of the reinforcement and of the concrete, respectively, and s is the interfacial slip, defined as the relative displacement between the two adherents (i.e. $s = u_r - u_b$). By means of Eqs. (11)–(15), it is possible to achieve the following second order differential equation in s:

$$\frac{d^2 s}{dx^2} - \frac{1+\rho}{E_r h_r} k_t s = 0 \tag{16}$$

where ρ is the mechanical fraction of reinforcement (i.e. $\rho = E_r t_r h_r / E_b t_b h_b$). Furthermore, observe that it is possible to express the stress in the FRP as a function of the first derivative of the slip:

$$\sigma_r = \frac{E_r}{1+\rho} \frac{ds}{dx} \tag{17}$$

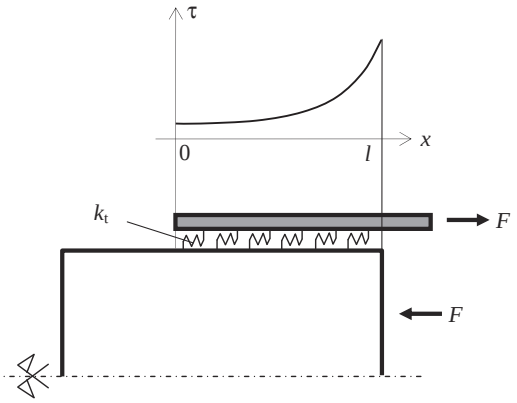

Fig. 5. Double pull–push shear test where the interface has been modeled as an elastic interface. Because of symmetry only the upper half has been drawn. The elastic shear stress field along the interface is evidenced.

Let us now introduce the characteristic length l_{ch} of the joint as:

$$l_{ch} = \sqrt{\frac{E_r h_r}{k_t(1+\rho)}} \tag{18}$$

which is essentially proportional to the square root of the ratio of the axial stiffness of the FRP plate to the tangential stiffness of the interface. Accordingly, Eq. (16) can be rewritten as:

$$\frac{d^2 s}{dx^2} - \frac{s}{l_{ch}^2} = 0 \tag{19}$$

The boundary conditions are $\sigma_r = 0$ for $x = 0$ and $\sigma_r = F/t_r h_r$ for $x = l$, respectively, F being the applied load (see Fig. 5). By means of Eq. (17) we can express the boundary conditions in terms of the relative displacement as:

$$\left.\frac{ds}{dx}\right|_{x=0} = 0 \tag{20}$$

$$\left.\frac{ds}{dx}\right|_{x=l} = \frac{(1+\rho)}{E_r t_r h_r} F \tag{21}$$

The final solution reads:

$$\tau(x,l) = k_t s = \frac{F}{t_r l_{ch}} \frac{\cosh(x/l_{ch})}{\sinh(l/l_{ch})} \tag{22}$$

which is also plotted in Fig. 5. It is evident that the stress distribution is not uniform: a stress concentration at the loaded end ($x = l$) occurs, where the shear stress attains its maximum value:

$$\tau(x = l, l) = \tau_{max} = \frac{F}{t_r l} \frac{l/l_{ch}}{\tanh(l/l_{ch})} \tag{23}$$

where the first ratio represents the shear stress averaged over the whole junction and the second ratio is the stress concentration factor. Note that, according to the present model, the peak shear stress occurs at the end of the overlap, which violates the stress-free condition at the edges of the adhesive layer. This is a common feature of the Volkersen-type models; it can be removed only by exploiting higher order models, which show that the peak takes place close to (but not at) the edge of the bond length.

If the failure of the interface were governed by strength, delamination would occur when the maximum shear stress Eq. (23) reaches the peak stress τ_p. Accordingly, the failure load $(F_c)_{str}$ becomes:

$$(F_c)_{str} = \tau_p t_r l_{ch} \tanh(l/l_{ch}) \tag{24}$$

Note that the stress criterion can only be applied to the weak interface model, since the stresses are unbounded in the case of strong interfaces.

On the other hand, if failure were governed by fracture energy, debonding would occur when the strain energy release rate reaches its critical value, i.e. the mode II fracture energy $\mathcal{G}_{IIc}$. By means of Eqs. (6) and (23), the failure load $(F_c)_{LEFM}$ according to LEFM can be easily recovered as:

$$(F_c)_{LEFM} = t_r l_{ch} \tanh(l/l_{ch}) \sqrt{2 k_t \mathcal{G}_{IIc}} = \tanh(l/l_{ch}) t_r \sqrt{\frac{2\mathcal{G}_{IIc} E_r h_r}{1+\rho}}. \tag{25}$$

Note that, if the interface is strong, the failure load provided by LEFM becomes:

$$F_c^{\infty} = t_r \sqrt{\frac{2\mathcal{G}_{IIc} E_r h_r}{1+\rho}} \tag{26}$$

and results to be independent of the bond length. The value (26) follows directly from Eq. (25) since, by letting the spring stiffness k_t go to infinity, l_{ch} (Eq. (18)) vanishes.

It is interesting to observe that, according to the weak interface model and to LEFM, the critical load (25) is monotonically increasing with the bond length. It vanishes for $l \to 0$, while for $l \to \infty$ it tends to the asymptotic value (26), which has therefore been denoted as F_c^∞. Note that $(F_c)_{LEFM}$ is always smaller than F_c^∞. This result is in agreement with what we observed in the previous section, i.e. the weak interface model usually provides failure loads smaller than the ones provided by the strong interface model.

The two failure loads estimates (24) and (25) can be cast in dimensionless form by dividing both sides by F_c^∞. Then, introducing the dimensionless length $\lambda = l/l_{ch}$, we get, respectively:

$$\frac{(F_c)_{LEFM}}{F_c^\infty} = \tanh(\lambda) \tag{27}$$

$$\frac{(F_c)_{str}}{F_c^\infty} = \frac{\tanh(\lambda)}{\sqrt{\mu}} \tag{28}$$

Since the dimensionless parameter μ is larger than unity, it is evident that the maximum shear stress criterion provides always lower values with respect to LEFM except for $\mu = 1$ (i.e. for linear elastic-perfectly brittle interfaces, see the thin line in Fig. 3), when the two predictions coincide. However, which estimate is more reliable? We will try to give an answer to this question on the basis of FFM in the following section.

4. Finite Fracture Mechanics applied to the pull–push shear test

According to the reference system shown in Fig. 5, Eq. (7) may be re-written as:

$$\begin{cases} \int_{l-\Delta}^{l} \tau(x,l)\,dx = \tau_p\,\Delta \\ \int_{l-\Delta}^{l} \frac{\tau^2(x=l',l')}{2k_t}\,dl' = \mathcal{G}_{IIc}\Delta \end{cases} \tag{29}$$

Upon substitution of Eqs. (22) and (23) into Eq. (29), we can integrate to obtain:

$$\begin{cases} \frac{F_c}{t_r}\left\{1 - \frac{\sinh[(l-\Delta)/l_{ch}]}{\sinh(l/l_{ch})}\right\} = \tau_p\Delta \\ \frac{F_c^2}{2k_t t_r^2 l_{ch}}\left[\frac{\Delta}{l_{ch}} - \coth\left(\frac{l}{l_{ch}}\right) + \coth\left(\frac{l-\Delta}{l_{ch}}\right)\right] = \mathcal{G}_{IIc}\Delta \end{cases} \tag{30}$$

which is a system of two equations in two unknowns: F_c, the critical load, and Δ, the crack advancement. By taking the ratio of the second equation to the square of the first one, we get an equation where the unique unknown is the dimensionless crack advancement $\delta = \Delta/l_{ch}$:

$$\delta\left[\frac{\sinh(\lambda)}{\sinh(\lambda) - \sinh(\lambda-\delta)}\right]^2 [\delta - \coth(\lambda) + \coth(\lambda-\delta)] = \mu \tag{31}$$

and the dimensionless parameter μ, defined previously by Eq. (9), appears at the right hand side. Eq. (31) can be easily solved numerically, looking for solutions within the range $0 < \delta < \lambda$. Once the value δ is found, we can obtain F_c either from the first or the second equation of the system (30). Choosing the first equation, the critical load F_c in dimensionless form reads:

$$\frac{F_c}{F_c^\infty} = \frac{\delta}{\sqrt{\mu}}\frac{\sinh(\lambda)}{\sinh(\lambda) - \sinh(\lambda-\delta)} \tag{32}$$

From Eqs. (31) and (32), it is evident that both the dimensionless load and the dimensionless crack advancement depend only on the two dimensionless parameters λ and μ. The former parameter, λ, is a function of the geometry of the problem and of the elastic properties of the adherents and of the adhesive, i.e. the interface; the latter one, μ, rules the brittleness/ductility of the interface.

The three predictions (27), (28) and (32) are plotted in Fig. 6 vs. the relative length λ for μ equal to 4, since, for FRP-to-concrete interfaces, typical μ values fall within the range 3–5, see, e.g., Yuan et al. (2004) or Mazzotti et al. (2009). It is evident that FFM yields predictions which are intermediate between the estimates provided by the energy (i.e. LEFM) and stress failure criteria. More in details, we can say that FFM is able to catch the transition between the strength-governed failure occurring for small bond lengths (for which $F_c/F_c^\infty \to \lambda/\sqrt{\mu}$) and the fracture energy-ruled failure taking place for large bond lengths (for which $F_c/F_c^\infty \to 1$). Note that the straight line of unit value corresponds to LEFM assuming perfect bonding (i.e. a strong interface).

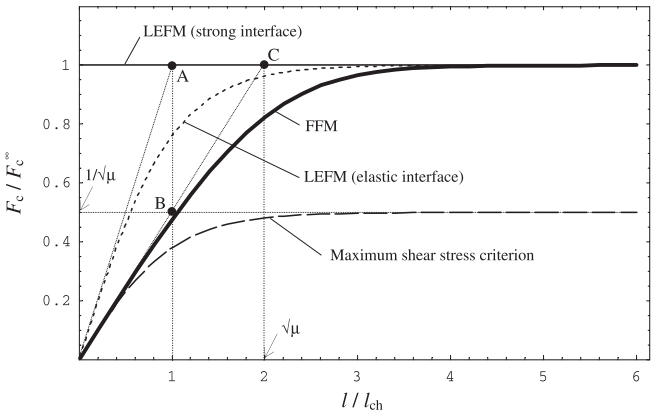

Fig. 6. Dimensionless failure load vs. dimensionless bond length according to different fracture criteria. The curves relative to FFM and maximum shear stress criterion are plotted assuming μ equal to 4, a typical value for FRP-to-concrete interfaces.

In Fig. 7 we plot the same graph for different values of the interface parameter μ, from 1 (corresponding to a linear elastic-perfectly brittle interface) to 8 (corresponding to an interface with a strong quasi-brittle behavior). As expected, the predictions provided by LEFM and the maximum shear stress criterion are very close for μ values close to unity, while they diverge as μ increases. On the other hand, FFM predictions lie always in between.

Since λ is usually rather large, FFM suggests that the predictions provided by LEFM should be considered more reliable with respect to the ones obtained by the maximum shear stress criterion. This remark justifies the application of LEFM (i.e. $\mathcal{G} = \mathcal{G}_c$) to delamination along elastic interfaces, the strain energy release rate being evaluated either by Eqs. (1) and (6) or (8), according to mode I, mode II or mixed mode delamination respectively (e.g., Bennati et al., 2009; Carpinteri et al., 2009; Távara et al., 2010). However, it should be highlighted that, for relatively short bond lengths (low λ values) and/or for interfaces with a remarkable quasi-brittle behavior (high μ values), LEFM overestimates the failure load, as clearly evidenced in Fig. 7. Therefore, its uncritical application is potentially dangerous. On the other hand, we believe that FFM provides accurate critical load estimates for a large range of bond lengths and of interface mechanical behaviors.

It is worth commenting about the knees of the LEFM, strength and FFM curves (points A, B and C in Fig. 6, respectively), defined as the points of intersection between the tangent at the origin and the asymptote at infinity. On the basis of Eqs. (27) and (28), it is straightforward to see that the abscissa of the points A and B is $\lambda = 1$ (corresponding to a bond length l equal to l_{ch}) regardless of the μ value (see also Fig. 7), while it increases to $\lambda = \sqrt{\mu}$ (corresponding to a bond length l equal to $l_{ch}\sqrt{\mu}$) for the FFM curve, point C. From Figs. 6 and 7, it is evident that the effective bond length l_e, defined as the bond length beyond which the load is approximately equal to its maximum F_c^∞, is roughly twice the length corresponding to the knee of the failure load vs. bond length curve, i.e. $l_e \cong (2/\tau_p)\sqrt{2\mathcal{G}_{IIc}E_r h_r/(1+\rho)}$. It means that the present approach predicts an increase of the effective bond length as the ductility of the interface increases, a feature Fig. 7 clearly highlights.

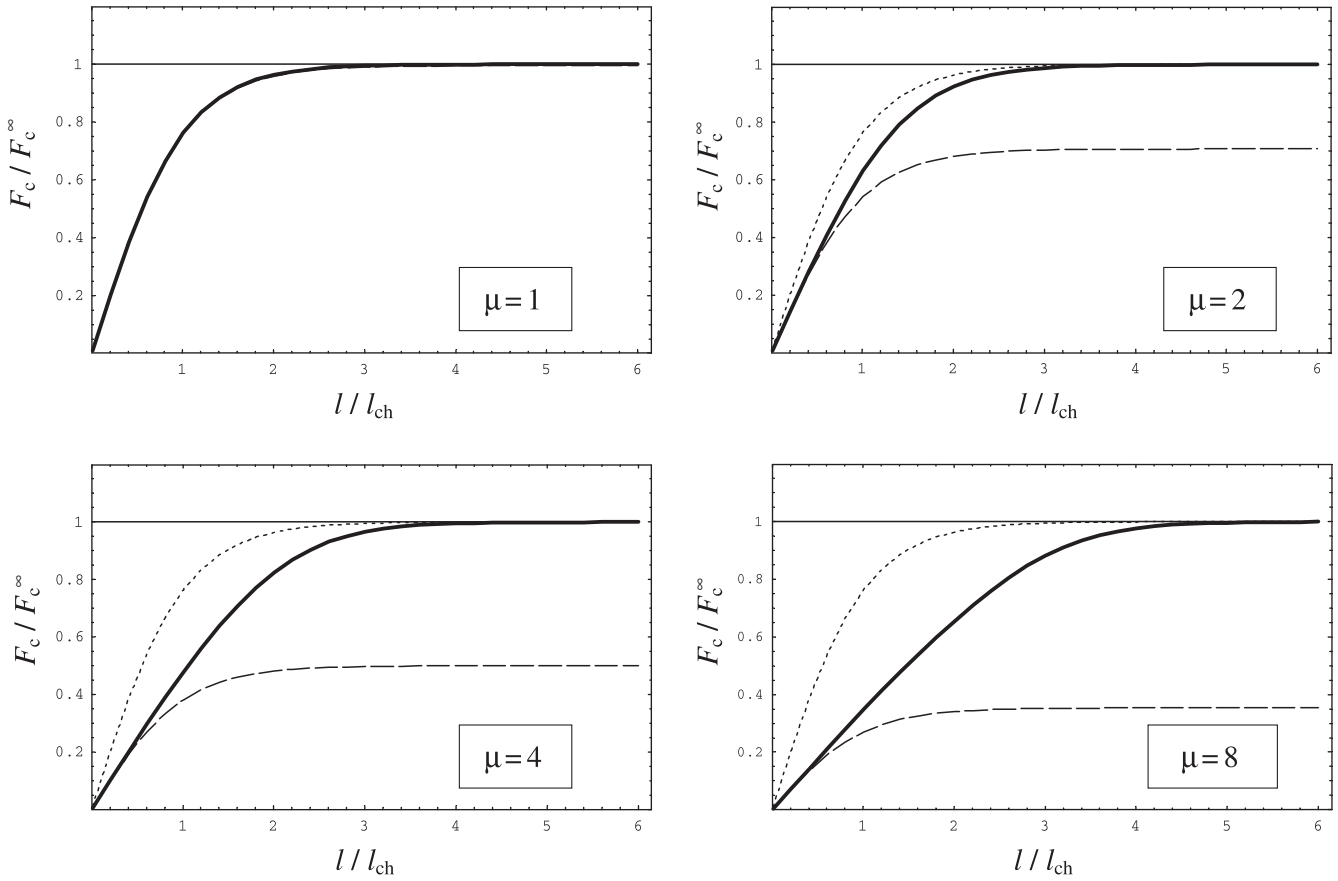

Fig. 7. Dimensionless load vs. dimensionless bond length for decreasing interface brittleness: from top left to bottom right, $\mu = 1, 2, 4, 8$. The thick lines represent the FFM predictions, the dashed lines correspond to the maximum shear stress criterion and the dotted lines to LEFM.

In Fig. 8a we plotted the dimensionless crack advancement δ vs. the dimensionless bond length λ for different μ values. Except for the case $\mu = 1$, when δ is always null since for a linear elastic-perfectly brittle interface FFM and LEFM coincide, for all the other admissible values ($\mu > 1$), the trend is the same: for short joints, Δ is proportional to the bond lengths, whereas it tends to a constant value for relatively large bond lengths. By Eq. (31) and some algebra, we can give an analytical expression to the asymptote for small bond lengths:

$$\delta = \frac{\mu - 1}{\mu}\lambda, \quad \text{for} \quad \lambda \to 0 \tag{33}$$

while the constant value δ^∞ attained for sufficiently large bond lengths is given by the solution of the following equation:

$$\frac{\delta}{1 - e^{-\delta}} = \sqrt{\mu}, \quad \text{for} \quad \lambda \to \infty \tag{34}$$

For the sake of clarity, in Fig. 8b we plotted also the relative crack increment, i.e. the ratio of the crack advancement Δ to the bond length l (which is also equal to δ/λ) vs. λ. In this case the curves show an initial value equal to $(\mu - 1)/\mu$ and then monotonically decrease down to zero for large lengths.

5. Comparison with other models

Wishing to check the soundness of the FFM approach to delamination along an elastic interface, we will compare its failure load estimates with the ones provided by the Cohesive Crack Model (CCM), whose capabilities to describe experimental data is widely recognized inside the scientific community (see, e.g., Carpinteri, 1989a,b).

In order to be implemented, usually the CCM needs a specific code. Indeed, one of the few cases that can be solved analytically, under the assumption of a cohesive law with a linear softening branch (see Fig. 3), is the pull–push shear test. Despite the simple geometry, the solution is relatively complicated, being characterized by five different stages: the elastic, the elastic-softening, the elastic-softening-debonding, the softening-debonding and the debonding stages. A complete description of such stages can be found in the papers by Yuan et al. (2004) and Cottone and Giambanco (2009) and, with a notation similar to the one used here, in Cornetti and Carpinteri (2011). Without entering into details, it can be proven that the maximum load is achieved in the elastic-softening stage. By imposing the stationary condition for the debonding load, the length l_{soft} of the process zone at peak load is provided by the following equation:

$$\sqrt{\mu - 1}\tanh(\lambda - \delta_{coh}) = \tan\left[\frac{\delta_{coh}}{\sqrt{\mu - 1}}\right] \tag{35}$$

where $\delta_{coh} = l_{soft}/l_{ch}$ is the dimensionless length of the process zone, i.e. the ratio of the portion of the bond length in the softening regime to the characteristic length given by Eq. (18). Eq. (35) is easily solved numerically; once δ_{coh} is evaluated, the failure load $(F_c)_{coh}$ is given by the following expression:

$$\frac{(F_c)_{coh}}{F_c^\infty} = \sqrt{\frac{\mu}{\mu - 1}}\sin\left[\frac{\delta_{coh}}{\sqrt{\mu - 1}}\right] \tag{36}$$

In Fig. 9 we compare the predictions obtained via FFM (Eq. (32)) and CCM (Eq. (36)) for different μ values. It is seen that they are

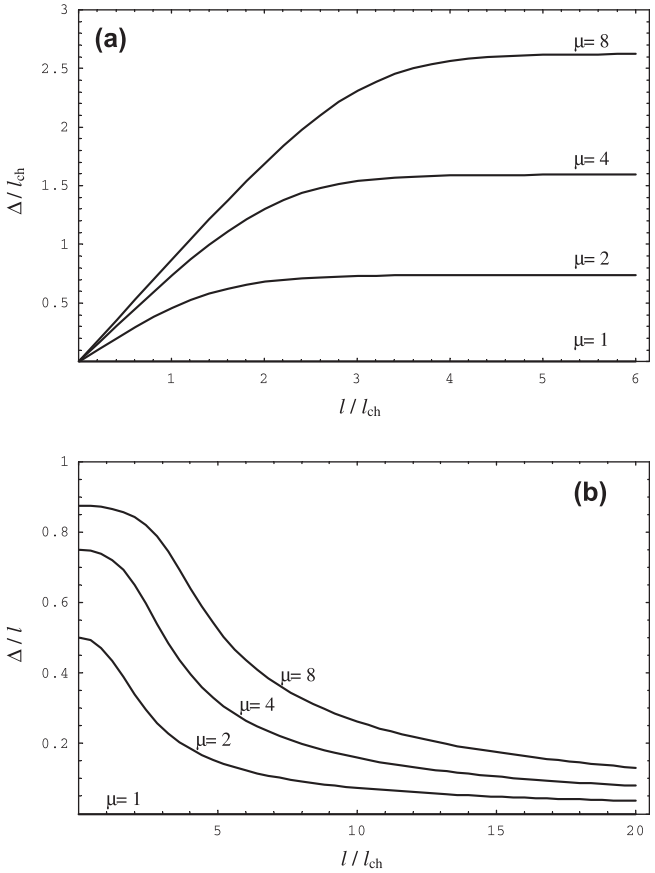

Fig. 8. Dimensionless crack advance vs. dimensionless bond length for different values of the interface parameter μ (a); ratio of the crack advancement to the bond length vs. dimensionless bond length for different value of the interface parameter μ (b).

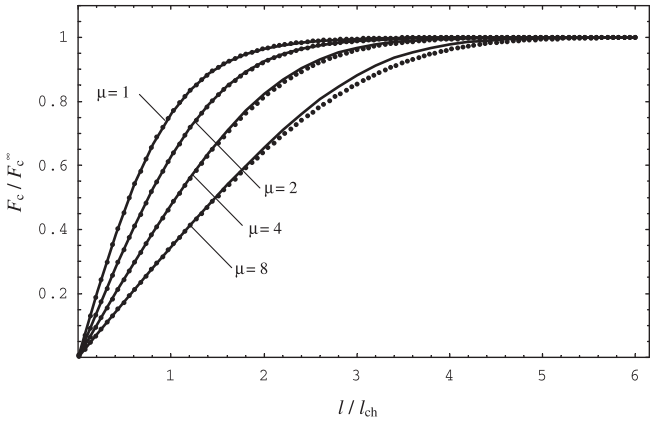

Fig. 9. Dimensionless load vs. dimensionless bond length for different interface brittleness: comparison between FFM (line) and CCM predictions (dots).

almost undistinguishable for relatively brittle interfaces (μ close to unity). On the other hand, FFM provides higher debonding load than CCM does for higher μ values. Nevertheless, it is evident that the two predictions remain very close each other even for interfaces with a strong softening behavior (e.g., $\mu = 8$).

In Fig. 10 we compared the crack advancement Δ according to FFM (Eq. (31)) and the length of the process zone at peak load according to the CCM (Eq. (35)). It is evident that the two lengths show the same trend: they are linearly increasing up to a certain bond length (the asymptote being the same, i.e. the one provided

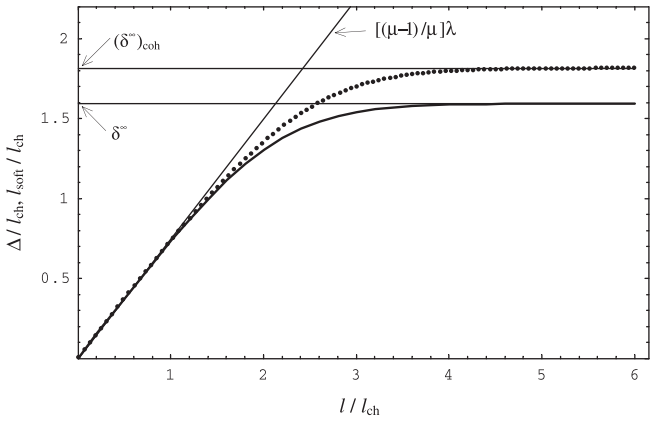

Fig. 10. Dimensionless crack advancement (according to FFM, continuous line) and dimensionless process zone (according to CCM, dots) vs. dimensionless bond length for $\mu = 4$.

by Eq. (33)) and then tend to a constant value, equal to δ^∞ according to FFM (Eq. (34)) and equal to $\delta^\infty_{\text{coh}}$ according to the CCM:

$$\delta^\infty_{\text{coh}} = \sqrt{\mu - 1}\arctan\left(\sqrt{\mu - 1}\right) \tag{37}$$

the latter value being slightly larger than the former one. Even if the two models remain distinct, it is evident that, by means of the finite crack advance of variable amplitude, FFM is able to catch the interplay between the size of the fracture process zone and the overall structural size (in this case represented by the joint length).

Although we analyzed only the pull–push geometry, we guess that the agreement between FFM and CCM (with linear softening) is a general feature, since both approaches require the same amount of energy to create fracture surfaces and make use of a length (either the crack advancement or the process zone) which is a structural parameter. Further analyses are needed to validate this argument. If confirmed, it would mean that, when we are interested only in the peak load, we may use FFM instead of the CCM. This can be of great advantage, since FFM requires only the elastic solution, while, as observed above, CCM needs a complete description of the loading process which, generally, has to be achieved by a suitable numerical procedure. Furthermore, FFM provides analytical results that can be exploited to develop formulae to be included in recommendations for engineering design.

While the ability of FFM to give accurate estimates of the failure load has been assessed, the debatable point is if FFM has a precise physical meaning and, therefore, if it is able to describe the post peak behavior as the CCM is. About the physics of the problem, we have shown that the crack increment Δ is closely correlated to the length of the process zone. However, for short bond lengths (low λ values) and ductile interfacial behavior (high μ values), the crack advancement is approaching the bond length (see Fig. 8b). In such a case, a strict application of FFM assumptions implies that complete detachment occurs in few discrete steps and, therefore, it may appear questionable. Moreover, averaging over almost the whole bond length may lead to lose some important information. On the other hand, we believe that FFM could successfully be applied to model saw-tooth like load-displacement plots occurring in certain experimental tests, as, for instance, the double cantilever beam test performed by Távara et al. (2010), to characterize a composite–composite joint for aeronautical applications. This investigation will be the subject of a future research.

Up to now we have shown that FFM and CCM are in excellent agreement. One could wonder if even easier failure criteria are able to provide similar results. To this aim, we now consider the average stress criterion, dating back to Neuber (1958) and Novozhilov

(1969), and the so-called point method proposed by Ritchie et al. (1973). For a review about these methods, see Taylor (2007), where these criteria are generally referred to as critical distance theories.

For what concerns the average stress criterion (called also line method, LM), the failure load is expected to occur when the average stress over a fixed length attains the shear strength τ_p. It is straightforward to prove that such a length (Δ_{LM}) must be given, in dimensionless form, by the solution of Eq. (34), denoted now by δ_{LM}. Eq. (32) provides the failure load as long as the variable crack advancement δ is replaced by δ_{LM} and the bond length l is larger then Δ_{LM} (i.e. $\lambda > \delta_{LM}$). For bond lengths shorter than Δ_{LM}, it is reasonable to average the stress over the whole bond length. Hence, the average stress criterion finally reads:

$$\frac{F_c}{F_c^\infty} = \frac{\lambda}{\sqrt{\mu}}, \quad \lambda \leqslant \delta_{LM} \tag{38}$$

$$\frac{F_c}{F_c^\infty} = \frac{\delta_{LM}}{\sqrt{\mu}} \frac{\sinh(\lambda)}{\sinh(\lambda) - \sinh(\lambda - \delta_{LM})}, \quad \lambda \geqslant \delta_{LM} \tag{39}$$

The point method (PM) states that failure occurs if the stress at a certain distance (Δ_{PM}) from the crack tip reaches the shear strength τ_p; as above, if Δ_{PM} exceeds l, we assume $\Delta_{PM} = l$. By denoting with δ_{PM} the ratio of Δ_{PM} to l_{ch} and exploiting the stress field of Eq. (22), the critical load according to the point method is:

$$\frac{F_c}{F_c^\infty} = \frac{\sinh(\lambda)}{\sqrt{\mu}}, \quad \lambda \leqslant \delta_{PM} \tag{40}$$

$$\frac{F_c}{F_c^\infty} = \frac{\sinh(\lambda)}{\sqrt{\mu}\cosh(\lambda - \delta_{PM})}, \quad \lambda \geqslant \delta_{PM} \tag{41}$$

where the critical distance has to be determined by imposing a failure load equal to F_c^∞ for infinite bond lengths in Eq. (41). Therefore:

$$\delta_{PM} = \frac{1}{2}\ln(\mu) \tag{42}$$

In Fig. 11a we plot the failure load estimates according to PM, LM, FFM and CCM. Although all the curves show the same slant and horizontal asymptotes for short and large bond lengths respectively, they are remarkably different in the middle, where they all exhibit a knee (Fig. 11b). By observing the plots, we can conclude that, for the problem under consideration, PM and LM are not so useful, at least for three reasons: (i) with respect to CCM, the PM and LM tend to overestimate the failure load significantly, i.e. up to 25 % and 15 % respectively (for $\mu = 5$, as assumed in Fig. 11), while the difference between FFM and CCM remains always below 2%; (ii) the two criteria shows some odd features without a clear physical meaning, i.e. the PM curve shows a concavity change while the LM shows a point where the first derivative is discontinuous (at $\lambda = \delta_{LM}$); (iii) most important, the critical distance (Δ_{LM} or Δ_{PM}, given in dimensionless form by Eq. (34) or (42), respectively) depends on l_{ch} (Eq. (18)), whose definition may vary from geometry to geometry. It means that the value of the critical distance is affected not only by the material parameters but also by the geometry of the problem.

The last observation represents a severe limitation to the advantages of using simple criteria such as the PM and LM in delamination problems. In fact the great advantage (and simplicity) of these criteria when applied to cracks or notches lying in a homogeneous media is that the critical distance is a pure material property and, therefore, a specific calculation for different geometries is not required. On the other hand, a proper calculation cannot be avoided in the present case. As a consequence, it is more convenient to apply directly FFM, which, being based on an energy balance, is physically more consistent and, at least in the present case, provides more accurate results (i.e. in better agreement with CCM).

Other critical distances approaches are the criteria based on a finite crack advance of constant length (Seweryn, 1998; Pugno and Ruoff, 2004; Taylor et al., 2005). It is easy to prove that, for delamination along a weak interface, they yield a zero or vanishing failure loads for bond lengths lower than or close to the finite crack advancement, respectively. Hence, for this specific problem, they are not reliable. The same (negative) conclusion holds for the effective crack approach (sometimes called equivalent-LEFM), where LEFM is applied to a crack length given by the actual one plus a material length.

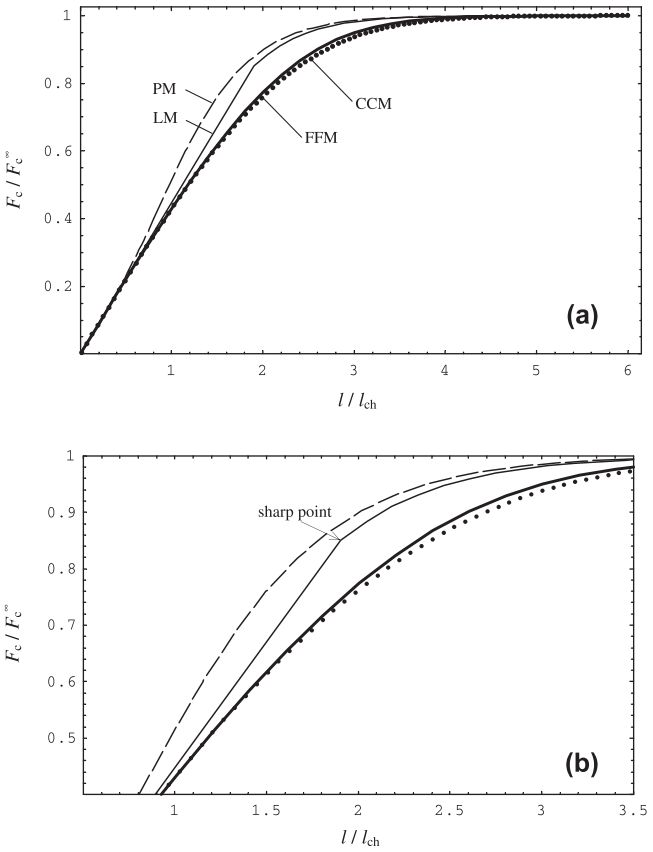

Fig. 11. Dimensionless load vs. dimensionless bond length according to different fracture criteria ($\mu = 5$): average stress, i.e. line method (LM, thin line), point method (PM, thin dashed line), FFM (thick line) and CCM (dots). Overall view (a); detail of the knee (b).

Finally, for what concerns the FFM criterion proposed by Leguillon (2002) (which differs from the present one because it is based on a point-wise stress condition), in the present case it provides estimates almost identical to those obtained by the PM. This is due to the fact that, while the crack advancement obtained using this criterion for very small λ coincides with that computed from Eq. (31), this crack advancement rapidly approaches δ_{PM} for increasing values of λ. Moreover, whereas the present FFM approach is in agreement with CCM with linear softening, preliminary results show that, at least for sufficiently large bond lengths, the FFM version proposed by Leguillon (2002) agrees with the predictions provided by a CCM where the cohesive stresses are constant up to a critical displacement (i.e. the Dugdale model, see Appendix A for details).

6. Conclusions

In the present paper we have developed a method to compute the critical load for a structure failing because of debonding along an interface. The method is based on the elastic interface model and on Finite Fracture Mechanics; it can be applied to cracked

and un-cracked geometries. With respect to LEFM, the present approach should provide better results for short or null pre-existing cracks and for interfaces with a remarkable softening behavior.

As an example, we applied the procedure to a relatively simple geometry, the pull–push shear test. The comparison with other fracture criteria points out the advantages of the present approach. Worthy of note is the excellent agreement with the Cohesive Crack Model.

The procedure outlined appears to be simple and general. It can be applied, for instance, to analyze delamination occurring in the double cantilever beam test for composite laminates or to model debonding of externally strengthened concrete beams. Further results could be obtained by properly extending the present approach to mixed mode delamination problems.

Acknowledgements

P.C. wishes to thank Professor David Taylor for useful discussions during the First IJFatigue & FFEMS Joint Workshop at Forni di Sopra (Italy) in March 2011. V.M. acknowledges the support by the Junta de Andalucía to the project "Proyecto de excelencia TEP-4051". P.C. and A.C. acknowledge the financial support of the Italian Ministry of Education, University and Research to the project "Advanced applications of fracture mechanics for the study of integrity and durability of materials and structures" within the PRIN program for the year 2008.

Appendix A

According to the FFM criterion proposed by Leguillon (2002), the failure of a pull–push shear specimen occurs whenever the following system is fulfilled:

$$\begin{cases} \tau(x = l - \Delta, l) = \tau_p \\ \int_{l-\Delta}^{l} \frac{\tau^2(x=l',l')}{2k_t}\,\mathrm{d}l' = \mathcal{G}_{IIc}\Delta \end{cases} \tag{A.1}$$

With respect to the criterion used in the present paper (Eq. (29)), it differs since it is based on a point-wise strength criterion instead of an average requirement. Upon substitution of Eqs. (22) and (23) into Eq. (A.1) and some analytical manipulations, one gets:

$$\left[\frac{\sinh(\lambda)}{\cosh(\lambda-\delta)}\right]^2 \frac{\delta - \coth(\lambda) + \coth(\lambda-\delta)}{\delta} = \mu \tag{A.2}$$

where the unique unknown is the dimensionless crack advancement δ. Although Eq. (A.2) has to be solved numerically, it can be shown that δ solution of (A.2) follows the asymptotic expression (33) for $\lambda \to 0$, while $\delta \to \delta_{PM}$ defined by Eq. (42) for $\lambda \to \infty$. The critical load is than obtained upon substitution of δ into the following expression:

$$\frac{F_c}{F_c^{\infty}} = \frac{\sinh(\lambda)}{\sqrt{\mu}\cosh(\lambda-\delta)} \tag{A.3}$$

On the basis of the analysis performed by Henninger et al. (2007) for a V-notch in a homogeneous medium, it is reasonable to expect that the predictions provided by (A.3) are in good agreement with an interface characterized by a Dugdale cohesive law (which assumes constant stresses up to the critical displacement). Hence, it is expected to be of little help in the description of FRP-to-concrete interfaces, where a strong softening is usually met, but could be useful for other structural joint analyses.

References

Andersons, J., Tarasovs, S., Spārniņš, E., 2010. Finite fracture mechanics analysis of crack onset at a stress concentration in a UD glass/epoxy composite in off-axis tension. Composites Science and Technology 70, 1380–1385.

Bennati, S., Colleluori, M., Corigliano, D., Valvo, P.S., 2009. An enhanced beam-theory model of the asymmetric double cantilever beam (ADCB) test for composite laminates. Composites Science and Technology 69, 1735–1745.

Benveniste, Y., Miloh, T., 2001. Imperfect soft and stiff interfaces in two-dimensional elasticity. Mechanics of Materials 33, 309–323.

Bigoni, D., Serkov, S.K., Valentini, M., Movchan, A.B., 1998. Asymptotic models of dilute composites with imperfectly bonded inclusions. International Journal of Solids and Structures 35, 3239–3258.

Bruno, D., Greco, F., 2001. Mixed mode delamination in plates: a refined approach. International Journal of Solids and Structures 38, 9149–9177.

Carpinteri, A., 1989a. Cusp catastrophe interpretation of fracture instability. Journal of the Mechanics and Physics of Solids 37, 567–582.

Carpinteri, A., 1989b. Post-peak and post-bifurcation analysis on cohesive crack propagation. Engineering Fracture Mechanics 32, 265–278.

Carpinteri, A., Cornetti, P., Pugno, N., 2009. Edge debonding in FRP strengthened beams: stress assessment versus fracture mechanics approach. Engineering Structures 31, 2436–2447.

Cornetti, P., Carpinteri, A., 2011. Modelling the FRP-concrete delamination by means of an exponential softening law. Engineering Structures 33, 1988–2001.

Cornetti, P., Pugno, N., Carpinteri, A., Taylor, D., 2006. Finite fracture mechanics: a coupled stress and energy failure criterion. Engineering Fracture Mechanics 73, 2021–2033.

Cottone, A., Giambanco, G., 2009. Minimum bond length and size effects in FRP-substrate bonded joints. Engineering Fracture Mechanics 76, 1957–1976.

Da Silva, L.F.M., das Neves, P.J.C., Adams, R.D., Spelt, J.K., 2009. Analytical models of adhesively bonded joints – Part I: literature survey. International Journal of Adhesion and Adhesives 29, 319–330.

England, A.H., 1965. A crack between dissimilar media. ASME Journal of Applied Mechanics 32, 400–402.

Goland, M., Reissner, E., 1944. The stresses in cemented joints. ASME Journal of Applied Mechanics 11, A17–A27.

Hart-Smith, L.J., 1973. Adhesive-bonded double-lap joints. NASA Contract Report 112235.

Hashin, Z., 2002. Thin interphase/imperfect interface in elasticity with application to coated composites. Journal of the Mechanics and Physics of Solids 50, 2509–2537.

Hebel, J., Dieringer, R., Becker, W., 2010. Modelling brittle crack formation at geometrical and material discontinuities using a finite fracture mechanics approach. Engineering Fracture Mechanics 77, 3558–3572.

Henninger, C., Leguillon, D., Martin, E., 2007. Crack initiation at a V-notch – comparison between a brittle fracture criterion and the Dugdale cohesive model. Comptes Rendu Mécanique 335, 388–393.

Kanninen, M.F., 1973. An augmented double cantilever beam model for studying crack propagation and arrest. International Journal of Fracture 9, 83–91.

Klarbring, A., 1991. Derivation of the adhesively bonded joints by the asymptotic expansion method. International Journal of Engineering Science 29, 493–512.

Leguillon, D., 2002. Strength or toughness? A criterion for crack onset at a notch. European Journal of Mechanics A/Solids 21, 61–72.

Leguillon, D., Laurencin, J., Dupeux, M., 2003. Failure initiation in an epoxy joint between two steel plates. European Journal of Mechanics A/Solids 22, 509–524.

Lenci, S., 2001. Analysis of a crack at a weak interface. International Journal of Fracture 108, 275–290.

Leung, C.K.Y., Yang, Y., 2006. Energy-based modelling approach for debonding of FRP plate from concrete substrate. Journal of Engineering Mechanics-ASCE 132, 583–593.

Mazzotti, C., Savoia, M., Ferracuti, B., 2009. A new single-shear set-up for stable debonding of FRP-concrete joints. Construction and Building Materials 23, 1529–1537.

Neuber, H., 1958. Theory of Notch Stresses. Springer-Verlag, Berlin.

Novozhilov, V., 1969. On a necessary and sufficient condition for brittle strength. Prikladnaya Matematika i Mekhanika 33, 212–222.

Pugno, N., Ruoff, R., 2004. Quantized fracture mechanics. Philosophical Magazine 84, 2829–2845.

Rabinovitch, O., 2004. Fracture-mechanics failure criteria for RC beams strengthened with FRP strips – a simplified approach. Composite Structures 64, 479–492.

Rice, J.R., 1988. Elastic fracture mechanics concepts for interfacial cracks. ASME Journal of Applied Mechanics 55, 98–103.

Rice, J.R., Sih, G.C., 1965. Plane problems of cracks in dissimilar media. ASME Journal of Applied Mechanics 32, 418–423.

Ritchie, R.O., Knott, J.F., Rice, J.R., 1973. On the relation between critical tensile stress and fracture toughness in mild steel. Journal of the Mechanics and Physics of Solids 21, 395–410.

Seweryn, A., 1998. A non-local stress and strain energy release rate mixed mode fracture initiation and propagation criteria. Engineering Fracture Mechanics 59, 737–760.

Suo, Z., Hutchinson, J.W., 1990. Interface crack between two elastic layers. International Journal of Fracture 43, 1–18.

Távara, L., Mantič, V., Graciani, E., Cañas, J., París, F., 2010. Analysis of a crack in a thin adhesive layer between orthotropic materials: an application to composite interlaminar fracture toughness test. Computer Modeling in Engineering and Sciences 58, 247–270.

Távara, L., Mantič, V., Graciani, E., París, F., 2011. BEM analysis of crack onset and propagation along fiber–matrix interface under transverse tension using a linear elastic–brittle interface model. Engineering Analysis with Boundary Elements 35, 207–222.

Taylor, D., 2007. The Theory of Critical Distances: A New Perspective in Engineering Fracture Mechanics. Elsevier, Oxford.
Taylor, D., Cornetti, P., Pugno, N., 2005. The fracture mechanics of finite crack extension. Engineering Fracture Mechanics 72, 1021–1038.
Volkersen, O., 1938. Die Nietkraftverteilung in Zugbeanspruchten Nietverbindungen mit Konstanten Laschen-querschnitten. Luftfahrtforschung, 15:4–47.
Weißgraeber, P., Becker, W., 2011. Predicting effective strengths of bonded lap joints with a finite fracture mechanics criterion. In: Fæster, S., Juul Jensen, D., Ralph, B., Sørensen, B.F. (Eds.). Proceedings of the 32nd Risø International Symposium in Materials Science "Composite materials for structural performance: Towards higher Limits". Technical University of Denmark, 5–9 September 2011, 479-486.
Williams, M.L., 1959. The stress around a fault or crack in dissimilar media. Bulletin of the Seismological Society of America, 49:199–204.
Yuan, H., Teng, J.G., Seracino, R., Wu, Z.S., Yao, J., 2004. Full-range behaviour of FRP-to-concrete bonded joints. Engineering Structures, 26: 553–565.